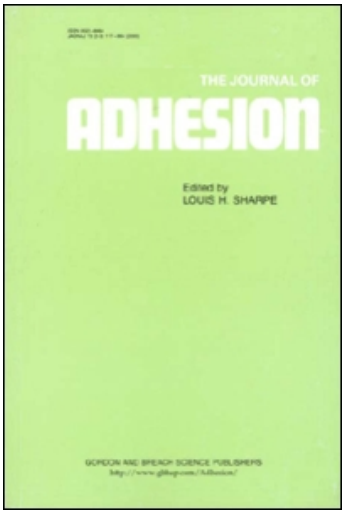

The Journal of Adhesion
Publication details, including instructions for authors and subscription information:
http://www.informaworld.com/smpp/title~content=t713453635

Mathematical Assessment of the Effects of Parabolic and Spherical Surface Topographies on the Interfacial State of Stress

Erol Sancaktar[a]; Weijian Ma[b]
[a] Polymer Engineering Department, University of Akron, Akron, OH, USA [b] Expro Engineering, Liverpool, NY, USA

To cite this Article Sancaktar, Erol and Ma, Weijian(2009) 'Mathematical Assessment of the Effects of Parabolic and Spherical Surface Topographies on the Interfacial State of Stress', The Journal of Adhesion, 85: 6, 302 — 323
To link to this Article: DOI: 10.1080/00218460902880156
URL: http://dx.doi.org/10.1080/00218460902880156

The Journal of Adhesion, 85:302–323, 2009

ISSN: 0021-8464 print/1545-5823 online
DOI: 10.1080/00218460902880156

Taylor & Francis
Taylor & Francis Group

Mathematical Assessment of the Effects of Parabolic and Spherical Surface Topographies on the Interfacial State of Stress

Erol Sancaktar[1] and Weijian Ma[2]
[1]Polymer Engineering Department, University of Akron, Akron, OH, USA
[2]Expro Engineering, Liverpool, NY, USA

A mathematical procedure to utilize the complementary energy method was developed, by minimization, in order to find an approximate analytical solution to the 3-D stress distributions in bonded interfaces of dissimilar materials. In order to incorporate the effects of surface topography, the interface was expressed as a general surface in Cartesian coordinates, i.e., F (x, y, z) = 0. The 3-D stress functions were used to produce 3-D stress components in dissimilar materials. At the interface, the internal tractions in each of the coordinate directions were balanced by the mathematical procedure. By using a penalty function method of the optimization theory, integration of the complementary energy produced the necessary equations to solve the 3-D stress distribution problem at the interface. A noticeable advantage of our method is that the stress jumps at the interface predicted in elasticity theory are captured, while standard finite element analysis (FEA) methods usually have difficulty to show such stress jumps at interfaces. The 3-D mathematical procedure we developed for obtaining the stress components at bonded bi-material interfaces offers significant promise in solving interface problems with different surface topographies, which can be described mathematically. Thus, the procedure developed provides an efficient tool to optimize interface construction by various methods such as chemical (etching), mechanical (machining, roughening, etc.), and other novel methods, such as laser ablation, currently becoming available to achieve desired interface stress distributions for bonded materials. In this paper, the parabolic interface problem, i.e., $y = x^2$, and the spherical interface problem, i.e., $y = x^2/4 + z^2/4$, are considered for an aluminum/epoxy interface.

Received 14 July 2008; in final form 19 January 2009.
Presented in part at the 2nd International Conference on Advanced Computational Engineering and Experimenting (ACE-X 2008), Barcelona, Spain, 14–15 July, 2008.
Address correspondence to Erol Sancaktar, Polymer Engineering Department, University of Akron, Akron, OH 44325-0301, USA. E-mail: erol@uakron.edu

Keywords: Adhesive joints; Bi-material interfaces; Bonding surfaces; Interface topographies; Interfacial stresses; Mechanical adhesion; Parabolic interfaces; Peel stresses; Shear stresses; Spherical interfaces; Stress jump; Surface roughening

1. INTRODUCTION

In order to design adhesive joints used in critical load bearing applications, it is necessary to have a detailed knowledge of the stress state and strength behavior of the joint. The finite element method and the continuum mechanics approach have been successfully applied to the analysis of adhesively bonded joints. A number of studies [1–6] have been carried out using the finite element method, which overcomes the difficulties arising from the geometrical complexity of bonded joints. Lap and butt joints have been analyzed extensively due to their common usage in engineering applications.

The need to produce more reliable and cost-effective joints demands a general design methodology along with the task of comparing the large array of adhesive joint configurations and determining which type of joint best suits the requirements. This study helps in developing a general methodology to compare adhesive joints for design optimization as well as giving us insight into the effects, on mechanical adhesion, of surface topography which can be considered a collection of many geometrical forms. For this purpose, the stress distributions were compared as functions of varying geometrical interfaces described mathematically in polynomial or other functional forms, as well as the material properties of the adhesive and the adherend or two different substrates joined by an infinitesimally thin adhesive layer.

Interfaces usually constitute a weak link in the chain of load transfer in bonded joints. Also, the discontinuity of the material properties causes abrupt changes in stress distribution, as well as causing stress singularities at the edges of the interfaces. It is very desirable to optimize the substrate surface topography at the interfaces to maximize the load bearing capacity of bonded joints, and to improve their deformational characteristics.

During the second half of the 20th century a considerable amount of research work has been published related to the interface stress distributions [7–28]. These studies focused on flat surfaces between two different materials except when the effects of surface roughness were investigated. In general, stress distributions, stress concentrations, singularities, and surface roughness effects were studied. These studies, however, were not extended to the development of a general methodology to include surface topography effects for varying

configurations which can be represented by different mathematical functions.

Recently, the finite element method has been successfully applied to the analysis of several different interface stress-strain phenomena. An investigation by Sancaktar and Narayan [29] on adhesively bonded scarf joints revealed that the angle between the bonded interface and the loading direction had a significant influence on the stress distributions at the interface.

Sawa and coworkers [30–34] conducted a number of investigations on the interface stress distribution in adhesively bonded butt joints under different loading conditions. The finite element method and the methods of elasticity based on stress functions were used in their studies. In most cases 2-dimensional (2-D) stresses were studied; in some cases, however, 3-dimensional (3-D) stress distributions were also investigated.

The finite element analysis (FEA) employs an averaging procedure from either side of the interface to arrive at interfacial stress values. Consequently, a single stress component common to both substrates, or the substrate and the adhesive, is reported for the interface. In order to be able to obtain separate stress components specific to each one of the bonded components on either side of the interface, FEA requires employment of the elemental nodes not on the interface, but on the next rows. This, however, presents a deficiency from the analysis point of view, since the theory of composite materials dictates that a stress jump occurs at bi-material interfaces. The mathematical procedure proposed here does not possess this deficiency.

The need to determine realistic stress distributions for bonded interfaces leading to interface optimization methodology to produce more reliable and cost-effective joints [35] demands complex mathematical treatments. For this purpose, a 3-D stress solution should be considered superior to a 2-D stress solution as it includes all of the stress components involved at the interface.

High levels of stresses result in crack propagation in brittle adhesives and cavitation-induced failures in deformable adhesives. Furthermore, not only the magnitudes but also the gradients of stresses and strains become an important issue in optimizing the joint strength. Large strain gradients at adhesive-substrate interfaces may result in bond failure [18,36].

Many researchers used FEA to investigate adhesive joints [37–39]. Penado and Dropek [37] used FEA for single, double lap, and scarf joints using four node quadrilateral plane strain elements. They considered the stresses in the middle row of elements in the adhesive. Sancaktar [18] and Baylor and Sancaktar [39] used FEA to execute

2-D stress analyses of single lap, scarf, and butt joints. They studied the effect of scarf angle on normal, shear, and transverse stress peaks and distributions.

In our previous papers [40,41], we provided example calculations using the 3-D mathematical procedure developed for obtaining the stress components at bonded bi-material interfaces and compared the results with the FEA results for the cases of flat ($y = 0$) and scarf ($y = x/2$) interfaces. Those works revealed that even though most of the stress distributions obtained were very similar to those obtained with the FEA method, our method also predicted the stress jumps at the interfaces, which could not be captured by the current FEA methods. Thus, we concluded that the novel mathematical procedure we developed offered significant promise in solving interface problems with different surface topographies, which can be described mathematically. This procedure not only provides 3-D stress information for the interfaces, but for the whole bonded component. The novelty of the procedure developed also includes the use of the penalty function to enforce the displacement boundary conditions at the interfaces. Furthermore, the mathematical procedure developed enables the integration of different interfacial topographies into the solution procedure, thus providing an efficient tool to optimize interface construction by various methods such as chemical (etching) [42], mechanical (machining, roughening, etc.) [42], and other novel methods, such as laser ablation [35], currently becoming available to achieve a desired interface stress distribution for bonded materials.

1.1. Purpose of the Study

This study attempts to describe the stress distribution on surfaces which form the interfaces between two different bonded materials, and can be described by the functional forms, $y = x^2$ (parabolic) and $y = x^2/4 + z^2/4$ (spherical). Many investigations have been performed in the past to evaluate the stress distribution, fracture, failure, and deformation behaviors of bonded joints with flat interfaces. However, no published work is available which evaluates the 3-D stress distribution on general interfaces with geometrical forms which can be expressed by polynomial or other mathematical functions. We believe that in order to understand the interfacial phenomena to optimize the load transfer characteristics of bonded joints and composite materials, in general, this type of mathematical formulation is necessary. For this purpose, the parabolic interface $y = x^2$ and the spherical interface $y = x^2/4 + z^2/4$ were investigated in this work.

For these purposes, approximate analytical expressions were developed for 3-D stress distributions at bonded interfaces of specific geometrical forms between substrates with different material properties, subjected to a tensile loading condition. We then developed a complementary energy method, which, when combined with an optimization method, enables the determination of the 3-D stress components. Thus, a computer program was constructed to evaluate the 3-D stress components using symbolic mathematic tools and numerical methods. For this purpose, MAPLE mathematical software (Maplesoft, Waterloo, Canada) was used, even though other commercial mathematical software packages can be equally employed. Finally, the methodology developed and the related computer program constructed were applied to the cases of parabolic, $y = x^2$, and the spherical, $y = x^2/4 + z^2/4$, interfaces.

1.2. Study Hypotheses

1. Linear elastic behavior was assumed throughout the study.
2. The interface was assumed to be perfectly bonded.
3. Stress singularities at the interface edges were not fully considered due to limitations with the computer capacity.
4. All force boundary conditions were fully imposed. The displacement boundary conditions, however, were limited in number to optimize the computational effort.
5. The complementary energy method rather than the potential energy method was used. The complementary energy method has been suggested to be superior to the potential energy method in determining the stress components, since it does not use derivatives to calculate the stresses as is done with the potential energy method [28].

2. THEORY AND ANALYTICAL PROCEDURES

2.1. Geometrical Representation of the Bonding Surface

The adherend surface to be bonded can be represented by any geometrical function,

$F(x,y,z) = 0$. Therefore, we have:

$$F_x = \partial F/\partial x, \quad F_y = \partial F/\partial y, \quad F_z = \partial F/\partial z, \tag{1}$$

which are proportional to the direction cosines of the normal to the surface $F(x, y, z) = 0$ at the point (x, y, z).

2.2. Three-Dimensional Stress Functions

The mathematical form of the 3-D stress functions should be chosen judiciously so as to be suitable for the intended application. This is done by choosing those functions which satisfy the boundary and compatibility conditions as well as the stress equilibrium conditions.

In order to find more suitable approximate solutions for stress distributions, we need to consider a variety of mathematical forms.

Three different functions were tested to improve the degree of approximation.

1. Hyperbolic

$$F1 = (w_1 + \cdots + w_5 x^4)\ \sinh(x) + (w_6 + \cdots + w_{10} x^4)\ \cosh(x) \quad (2)$$

2. Trigonometric:

$$F2 = w_1\ \sin(x) + w_2\ \cos(x) + \cdots + w_9\ \sin(5x) + w_{10}\ \cos(5x) \quad (3)$$

3. Exponential:

$$F3 = w_1 e^{x} + w_2 e^{-x} + w_3 e^{2x} + w_4 e^{-2x} + \cdots + w_9 e^{5x} + w_{10} e^{-5x} \quad (4)$$

For initial analysis, the above three functions were used to approximate the functions 1, x, $\sin(\pi x)$, $\cos(\pi x)$, $e^{3x/2}$, and $\ln[(2/5) - x^2]$ in the interval $[(-1/2), (1/2)]$. The terms $3/2$ and $2/5$ in the exponential and logarithmic functions, respectively, were chosen arbitrarily. The calculation method was as follows. Take ten points evenly distributed in the interval including both ends. At each point, we make the approximating function equal to the original function. Therefore, we obtain ten linear equations. Solving the ten linear equations together, the values of w_1, w_2,..., w_{10}, can be found, and the approximating function can be established. Our comparative calculations revealed that F1 is suitable for approximation purposes.

To satisfy the compatibility conditions, the principle of minimization of the complementary energy of the two-material system was used. Following the variational principle of elasticity, the approximate analytical solution was obtained. As the number of terms in the polynomial stress functions increases, the solution should closely approximate the exact case.

2.3. Boundary Conditions

To solve the stress distribution problem for the bonded joint, the boundary conditions need to be defined first. The correct solution should satisfy the stress and force equilibrium conditions on the surfaces of the

two-body system including the interface $F(x, y, z) = 0$. The continuity of displacements needs to be enforced at the interface area.

For stress balance at the interface, $F(x, y, z) = 0$, we have:

$$\sigma^A_{xx}F_x + \sigma^A_{xy}F_y + \sigma^A_{xz}F_z = \sigma^B_{xx}F_x + \sigma^B_{xy}F_y + \sigma^B_{xz}F_z \tag{5}$$

$$\sigma^A_{xy}F_x + \sigma^A_{yy}F_y + \sigma^A_{yz}F_z = \sigma^B_{xy}F_x + \sigma^B_{yy}F_y + \sigma^B_{yz}F_z \tag{6}$$

$$\sigma^A_{xz}F_x + \sigma^A_{yz}F_y + \sigma^A_{zz}F_z = \sigma^B_{xz}F_x + \sigma^B_{yz}F_y + \sigma^B_{zz}F_z, \tag{7}$$

where A and B define the two different material regions with A corresponding to the substrate, and B to the adhesive bonded at the interface, and the stress components, σ_{ij}, are defined based on the Cartesian system of Fig. 1.

The continuity of displacement is enforced at the interface area using the fundamental theorem for surface theory of differential geometry [43] instead of directly using displacements. This way, the integrations of displacements are avoided, and the stress distribution can be calculated more accurately.

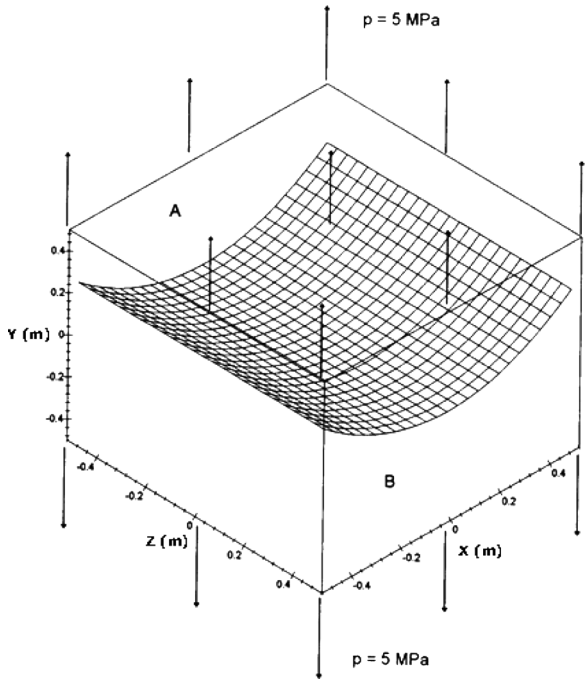

FIGURE 1 Geometry and loading pattern used in the analysis for the parabolic ($y = x^2$) interface.

Let ds = (dx, dy, dz) be any line element on the undeformed interface, and ds' the deformed line element of ds. On the interface we have $dy = F_x\,dx + F_z\,dz$. Then,

$$[(ds')^2 - (ds)^2]/(ds)^2 = e_{xx}l^2 + e_{yy}m^2 + e_{zz}n^2 + 2e_{xy}ml + 2e_{xz}nl + 2e_{yz}mn, \tag{8}$$

where, e_{xx}, e_{yy}, e_{zz}, e_{xy}, e_{xz}, and e_{yz} are the strain components, and l, m, and n are the initial direction cosines of the line element, ds. We call the $(ds')^2$ the first fundamental form of the deformed interface.

Because ds is at the interface, each line element at the interface belongs to both regions, and thus $(ds')^2$ should be the same for both the Materials A and B. Then, we have

$$e^A_{xx} + 2e^A_{xy}F_x + e^A_{yy}F_x^2 = e^B_{xx} + 2e^B_{xy}F_x + e^B_{yy}F_x^2 \tag{9}$$

$$e^A_{zz} + 2e^A_{yz}F_z + e^A_{yy}F_z^2 = e^B_{zz} + 2e^B_{yz}F_z + e^B_{yy}F_z^2 \tag{10}$$

$$e^A_{xy}F_z + e^A_{yz}F_x + e^A_{yy}F_xF_z + e^A_{xz} = e^B_{xy}F_z + e^B_{yz}F_x + e^B_{yy}F_xF_z + e^B_{xz}, \tag{11}$$

where e^A_{ij} and e^B_{ij} are strain components of Materials A and B, respectively.

At the interface the corresponding components of the partial derivatives of rotation with respect to x and z should be the same at any point. Therefore, we must have:

$$\begin{aligned}(\partial e^A_{xz}/\partial y) - (\partial e^A_{xy}/\partial z) + F_x\left[(\partial e^A_{yz}/\partial y) - (\partial e^A_{yy}/\partial z)\right] \\ = (\partial e^B_{xz}/\partial y) - (\partial e^B_{xy}/\partial z) + F_x\left[(\partial e^B_{yz}/\partial y) - (\partial e^B_{yy}/\partial z)\right]\end{aligned} \tag{12}$$

$$\begin{aligned}(\partial e^A_{xx}/\partial z) - (\partial e^A_{xz}/\partial x) + F_x\left[(\partial e^A_{xy}/\partial z) - (\partial e^A_{yz}/\partial x)\right] \\ = (\partial e^B_{xx}/\partial z) - (\partial e^B_{xz}/\partial x) + F_x\left[(\partial e^B_{xy}/\partial z) - (\partial e^B_{yz}/\partial x)\right]\end{aligned} \tag{13}$$

$$\begin{aligned}(\partial e^A_{xy}/\partial x) - (\partial e^A_{xx}/\partial y) + F_x\left[(\partial e^A_{yy}/\partial x) - (\partial e^A_{xy}/\partial y)\right] \\ = (\partial e^B_{xy}/\partial x) - (\partial e^B_{xx}/\partial y) + F_x\left[(\partial e^B_{yy}/\partial x) - (\partial e^B_{xy}/\partial y)\right]\end{aligned} \tag{14}$$

$$\begin{aligned}(\partial e^A_{zz}/\partial y) - (\partial e^A_{yz}/\partial z) + F_z\left[(\partial e^A_{yz}/\partial y) - (\partial e^A_{yy}/\partial z)\right] \\ = (\partial e^B_{zz}/\partial y) - (\partial e^B_{yz}/\partial z) + F_z\left[(\partial e^B_{yz}/\partial y) - (\partial e^B_{yy}/\partial z)\right]\end{aligned} \tag{15}$$

$$\begin{aligned}(\partial e^A_{xz}/\partial z) - (\partial e^A_{zz}/\partial x) + F_z\left[(\partial e^A_{xy}/\partial z) - (\partial e^A_{yz}/\partial x)\right] \\ = (\partial e^B_{xz}/\partial z) - (\partial e^B_{zz}/\partial x) + F_z\left[(\partial e^B_{xy}/\partial z) - (\partial e^B_{yz}/\partial x)\right]\end{aligned} \tag{16}$$

$$\begin{aligned}(\partial e^{A}_{yz}/\partial x) - (\partial e^{A}_{xz}/\partial y) + F_z\left[(\partial e^{A}_{yy}/\partial x) - (\partial e^{A}_{xy}/\partial y)\right] \\ = (\partial e^{B}_{yz}/\partial x) - (\partial e^{B}_{xz}/\partial y) + F_z\left[(\partial e^{B}_{yy}/\partial x) - (\partial e^{B}_{xy}/\partial y)\right]\end{aligned} \quad (17)$$

We will refer to the above relationships (12–17) as "the second fundamental form of the deformed interface." According to the fundamental theorem for surface theory of differential geometry, we can say that, "if first and second fundamental forms have been predetermined, then a surface is uniquely determined except for its position in space."

The continuity of displacement is enforced at the interface area. For the complementary energy formulation, the variation of complementary energy, δI, can be described as:

$$\delta I = \delta\xi - \int_{S1} u_i^{S1}\delta p_i^{S1}\, dS - \int_{S2} u_i^{S2}\delta p_i^{S2}\, dS - \int_{Si} u_i^{A}\delta p_i^{A}\, dS - \int_{Si} u_i^{B}\delta p_i^{B}\, dS. \quad (18)$$

The function ξ is the complementary energy defined by

$$\xi = \int_V \xi_0\, dV, \quad (19)$$

where ξ_0 is called the complementary energy density defined by

$$\xi_0 = -U_0 + \sigma_{ij}e_{ij}. \quad (20)$$

The U_o function is the strain energy density:

$$U_0 = \frac{1}{2}\sigma_{ij}e_{ij} = \frac{1}{2}C_{ijkl}e_{ij}e_{kl}, \quad (21)$$

where the elastic constants C_{ijk1} are the components of a Cartesian tensor of the fourth order.

We divide the outside boundary surface, S, into two zones, S_1 and S_2. On S_1 the traction components p_i^{S1} are specified so that $\delta p_i^{S1} = 0$, while on S_2 the displacements u_i^{S2} are specified. The S_i is the interface between the two different materials, where u_i^A, u_i^B and p_i^A, p_i^B are displacements and traction forces on each material interface, respectively. From the interface stress balance just mentioned above, we have $p_i^A = -p_i^B$, and we obtain

$$\delta I = \delta\xi - \int_{S_2} u_i^{s2}\delta p_i^{s2}\, dS - \int_{Si} (u_i^A - u_i^B)\delta p_i^A\, dS. \tag{22}$$

Let $u_i^A = u_i^B$, then

$$\delta I = \delta\xi - \int_{S_2} u_i^{s2}\delta p_i^{s2}\, dS. \tag{23}$$

When no external displacement boundary conditions are specified, S_2 is a zero set, and we have

$$\delta I = \delta\xi. \tag{24}$$

Thus, we have imposed both the force and displacement boundary conditions at the interface.

Based on the above discussions, we assume that the deformed interfaces of Materials A and B are identical, and S_2 is zero. Furthermore, we note that due to computational difficulty, the condition of displacement match between the Bodies A and B at the interface could not be done exactly. The deformed interfaces will match approximately by minimization of compatibility conditions in Bodies A and B, and by the employment of the penalty function to minimize any interfacial displacement mismatch numerically. This will be further explained in Section 2.4.1.

2.4. Compatibility Equations

Elasticity principles dictate that any stress distribution should satisfy the compatibility equations. If 3-D stress functions are used in conjunction with the variational method and the complementary energy method, it can be shown [44–46] that the six compatibility equations are automatically satisfied when the complementary energy reaches its minimum value.

2.4.1. Minimization of the Complementary Energy Function Using Penalty Functions

In the above discussion, we proposed the minimization of the complementary energy function because it had a positive defined quadratic form. By using the Newton quadratic optimization method [47] we can easily find the minimum point. In order to find the minimum solution of $f(x)$, which is subjected to $g_i(x) \geq 0,\ i = 1, 2, \ldots, n$ and $h_j(x) = 0,\ j = 1, 2, \ldots, m$, we want to use the penalty function method [48]. The penalty function method requires users to form a special function $p(x, R) = f(x) + \Omega[R, g(x), h(x)]$, where R is a set of

penalty parameters and Ω is a function of R, g(x), and h(x). The exact way in which the Ω is formed depends on different situations.

One specific form of the Ω function is $\Omega = [h(x)]^2 R$ in the absence of the g(x) terms. This yields $p(x, R) = f(x) + [h(x)]^2 R$. Notice that the parameter R equally discourages positive or negative violations of $h(x) = 0$. In addition, it is clear that with increasing values of R the stationary values of p(x, R) will reach x^m, since, in the limit, as R grows large, $h(x) \to 0$.

To find the minimum value of the complementary energy subjected to the condition $u_i^A = u_i^B$, at the interface, we can construct a function

$$\Pi = I + R \sum_{i=1\ldots3}^{y=f(x,z)} (u_i^A - u_i^B)^2, \tag{25}$$

where R has a very large positive value. Since I has a minimum value and a quadratic form, and $R \sum_{i=1\ldots3}^{y=f(x,z)} (u_i^A - u_i^B)^2$ is positive defined, Π also has a minimum value and a quadratic form.

Consequently, using the Newton quadratic method, we can find an approximate solution to minimize the complementary energy of the two-body system subjected to the interface geometry boundary conditions. To choose the R, it was found that the R must be large enough to impose the interface displacement matching, by satisfying Eqs. (9–17) using the least squares approximation, as well as minimization of the complementary energy, while not causing a big change in the complementary energy of the total system. For this purpose an iterative scheme was used with the initial value $R = 0$. Subsequent to its second value of unity, the R value was increased by tenfold in subsequent increments until the change in the complementary energy was larger by about 0.1%, which was chosen arbitrarily for numerical expediency. For the work reported in this article, this iteration resulted in the R value of 10^6.

2.5. Summary of the Proposed Mathematical Procedure

The following steps were used to obtain the stress distributions:

1. Choose the appropriate stress functions, Φ_{mn}, to satisfy stress boundary conditions.
2. Relate the stress functions, Φ_{mn}, to the stress distribution functions, σ.
3. Use stress interface boundary conditions, Eqs. (5–7), to reduce the unknown variables in the stress distribution functions obtained.
4. Define a function Π according to Eq. (25). Π is the sum of the complementary energy I, and the penalty function, $R \sum_{i=1\ldots3}^{y=f(x,z)}$

$(u_i^A - u_i^B)^2 R$, was chosen such that it is the largest positive number which causes the total system complementary energy to change by only 0.1%

5. Use the remaining unknown variables to minimize the function Π formed in Step 4, and solve all the unknown variables to obtain the complete stress distribution functions.

3. RESULTS AND DISCUSSION

The coordinate system used is shown in Fig. 1.

3.1. General Form of the Stress Functions

The stress functions used are given by the following general equations:

$$\Phi_{xx}^A = [z^2 - (1/4)]^2[y - (1/2)]^2 f_1(x, y, z) \tag{26}$$

$$\Phi_{yy}^A = [z^2 - (1/4)]^2[x^2 - (1/4)]^2 f_2(x, y, z) \tag{27}$$

$$\Phi_{zz}^A = [x^2 - (1/4)]^2[y - (1/2)]^2 f_3(x, y, z) \tag{28}$$

$$\Phi_{xy}^A = [x^2 - (1/4)][z^2 - (1/4)]^2[y - (1/2)] f_4(x, y, z) \tag{29}$$

$$\Phi_{xz}^A = [x^2 - (1/4)][z^2 - (1/4)][y - (1/2)]^2 f_5(x, y, z) \tag{30}$$

$$\Phi_{yz}^A = [x^2 - (1/4)]^2[z^2 - (1/4)][y - (1/2)] f_6(x, y, z) \tag{31}$$

$$\Phi_{xx}^B = [z^2 - (1/4)]^2[y + (1/2)]^2 f_7(x, y, z) \tag{32}$$

$$\Phi_{yy}^B = [z^2 - (1/4)]^2[x^2 - (1/4)]^2 f_8(x, y, z) \tag{33}$$

$$\Phi_{zz}^B = [x^2 - (1/4)]^2[y + (1/2)]^2 f_9(x, y, z) \tag{34}$$

$$\Phi_{xy}^B = [x^2 - (1/4)][z^2 - (1/4)]^2[y + (1/2)] f_{10}(x, y, z) \tag{35}$$

$$\Phi_{xz}^B = [x^2 - (1/4)][z^2 - (1/4)][y + (1/2)]^2 f_{11}(x, y, z) \tag{36}$$

$$\Phi_{yz}^B = [x^2 - (1/4)]^2[z^2 - (1/4)][y + (1/2)] f_{12}(x, y, z). \tag{37}$$

3.2. Application for the Parabolic ($y = x^2$) Interface

The interface $y = x^2$ is shown in Fig. 1. For the parabolic interface, the functions $f_n(x, y, z)$ are of the type:

$$\begin{aligned} f_n(x, y, z) = {} & g_{n1} \sin h(x) \sin h(z) + g_{n2} \sin h(x) \cos h(z) \\ & + g_{n3} \cos h(x) \sin h(z) + g_{n4} \cos h(x) \cos h(z), \end{aligned} \tag{38}$$

where g_{ni} are defined by:

$$g_{ni} = h_{ni1} + h_{ni2}x + h_{ni3}z. \tag{39}$$

h_{ni1}, h_{ni2}, and h_{ni3} are polynomials of $[a_{nij1} + \ldots + a_{nijm}\ (y - x^2)^{m-1}]$, where a_{nijk} are the constants of the polynomial. Figures 2–5 show the stresses σ_{xx} (Fig. 2), σ_{yy} (Fig. 3), σ_{zz} (Fig. 4), and σ_{xz} (Fig. 5), (a) on the epoxy adhesive (Body B) and (b) on the aluminum substrate (Body A) for each figure at the parabolic bi-material interface, as calculated by the mathematical procedure. As illustrated by comparisons of the stresses in each of these figures, stress jumps are observed in all of the interfacial stress distributions with transition between Bodies A and B. We note that since the stress distributions are plotted in reference to the global coordinate system (see Fig. 1), the fact that the interface is varying as $y = x^2$ function with respect to the global y and x axes affects the presence and the magnitude of these stress jumps. For example, for σ_{yy} (Fig. 3), the stress jump observed between Bodies A and B is solely due to this coordinate transformation as force balance is maintained between Bodies A and B in the direction perpendicular to the interface. However, we should also note that the "stress jump" is a real physical phenomenon for bonded interfaces and it is observed for transverse stresses σ_{xx}, σ_{zz}, and for the shear stress σ_{xz}, even in the case of flat interfaces, which are perpendicular to the applied distributed loads (Fig. 1), as illustrated in our earlier work [40].

The stresses σ_{xy} and σ_{yz} on the epoxy adhesive (Body B) at the parabolic bi-material interface, as calculated by the mathematical procedure, are shown in Fig. 6.

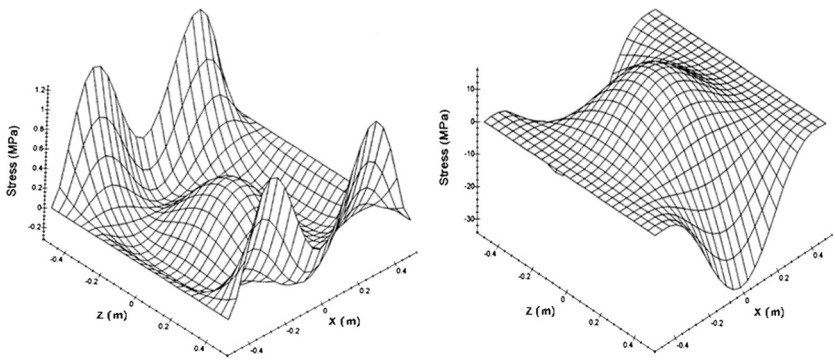

(a) (b)

FIGURE 2 Stress σ_{xx}, (a) on the epoxy adhesive (Body B) and (b) on the aluminum substrate (Body A) at the parabolic bi-material interface, as calculated by the mathematical procedure.

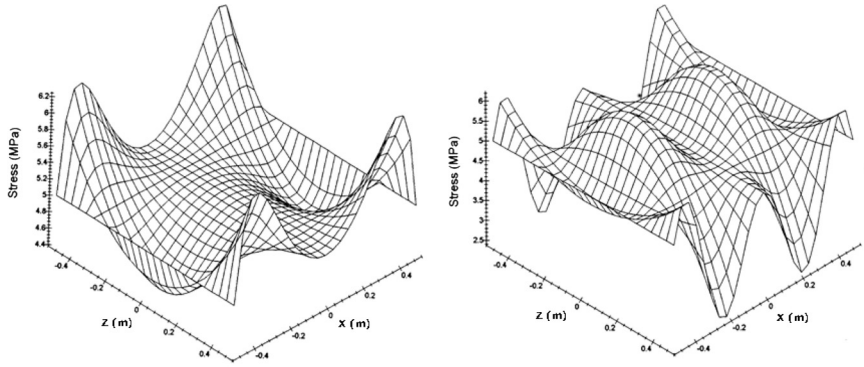

FIGURE 3 Stress σ_{yy}, (a) on the epoxy adhesive (Body B) and (b) on the aluminum substrate (Body A) at the parabolic bi-material interface, as calculated by the mathematical procedure.

3.3. Application for the Spherical $(x^2 + (y-2)^2 + z^2 = 4)$ Interface

The spherical interface $x^2 + (y-2)^2 + z^2 = 4$ can be approximately expressed by polynomial $y = x^2/4 + z^2/4$, and it is shown in Fig. 7. Therefore, all of the functions f_n (x, y, z) are of the type:

$$\begin{aligned} f_n(x,y,z) = {} & g_{n1}\sinh(x)\sinh(z) + g_{n2}\sinh(x)\cosh(z) \\ & + g_{n3}\cosh(x)\sinh(z) + g_{n4}\cosh(x)\cosh(z), \end{aligned} \tag{38}$$

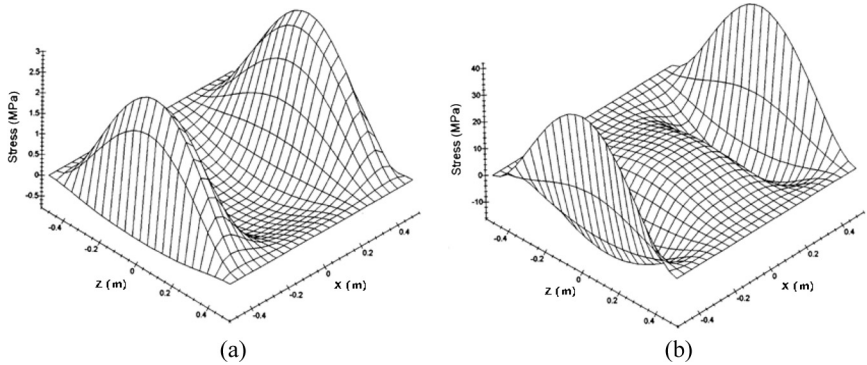

FIGURE 4 Stress σ_{zz}, (a) on the epoxy adhesive (Body B) and (b) on the aluminum substrate (Body A) at the parabolic bi-material interface, as calculated by the mathematical procedure.

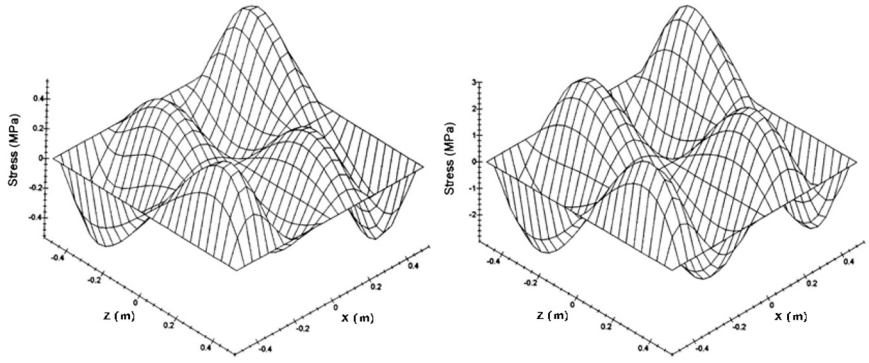

FIGURE 5 Stress σ_{xz}, (a) on the epoxy adhesive (Body B) and (b) on the aluminum substrate (Body A) at the parabolic bi-material interface, as calculated by the mathematical procedure.

where g_{ni} are defined by:

$$g_{ni} = h_{ni1} + h_{ni2}x + h_{ni3}z. \tag{39}$$

h_{ni1}, h_{ni2} and h_{ni3} are polynomials of $\{a_{nij1} + \cdots + a_{nijm}\ [y - (x^2/4) - (z^2/4)]\}$, where a_{nijk} are the constants of the polynomial. Figures 8–11 show the stresses σ_{xx} (Fig. 8), σ_{yy} (Fig. 9), σ_{zz} (Fig. 10), and σ_{xz} (Fig. 11), (a) on the epoxy adhesive (Body B) and (b) on the aluminum substrate (Body A) for each figure at the spherical bi-material

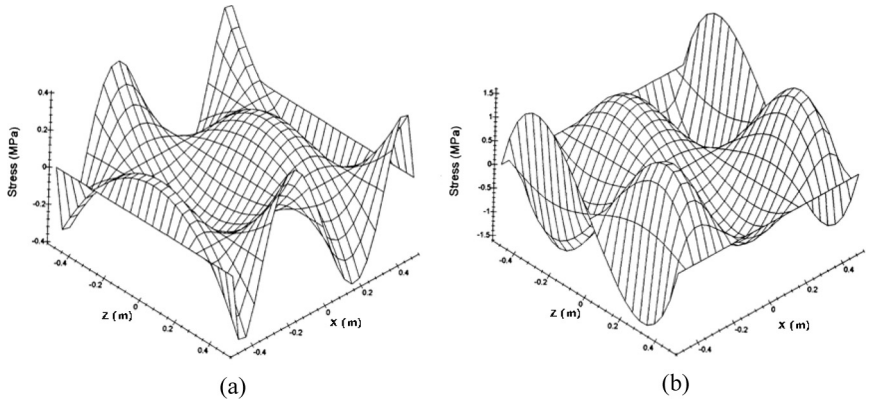

FIGURE 6 Stresses (a) σ_{xy} and (b) σ_{yz} on the epoxy adhesive (Body B) at the parabolic bi-material interface, as calculated by the mathematical procedure.

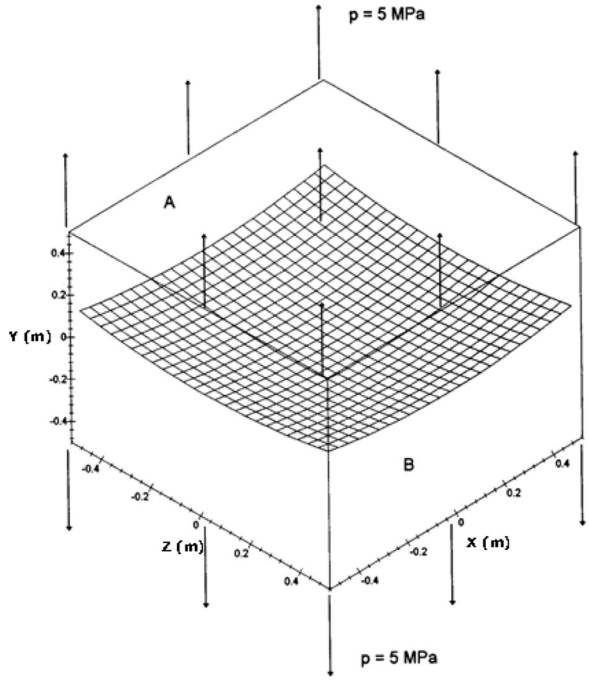

FIGURE 7 Geometry and loading pattern used in the analysis for the spherical $(x^2 + [y-2]^2 + z^2 = 4)$ interface.

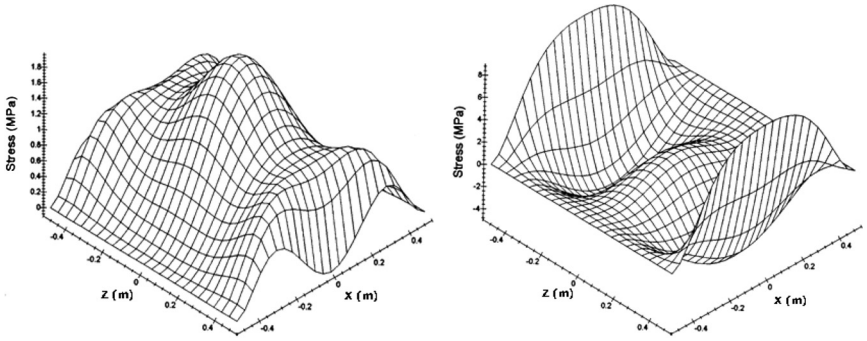

(a) (b)

FIGURE 8 Stress σ_{xx}, (a) on the epoxy adhesive (Body B) and (b) on the aluminum substrate (Body A) at the spherical bi-material interface, as calculated by the mathematical procedure.

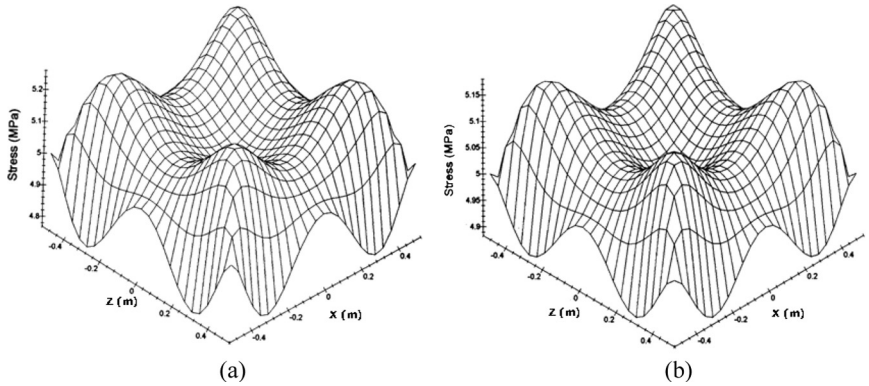

FIGURE 9 Stress σ_{yy}, (a) on the epoxy adhesive (Body B) and (b) on the aluminum substrate (Body A) at the spherical bi-material interface, as calculated by the mathematical procedure.

interface, as calculated by the mathematical procedure. As illustrated by comparisons of the stresses in each of these figures, stress jumps are again observed in all of the interfacial stress distributions with transition between Bodies A and B.

The stresses σ_{xy} and σ_{yz} on the epoxy adhesive (Body B) at the spherical bi-material interface, as calculated by the mathematical procedure, are shown in Fig. 12.

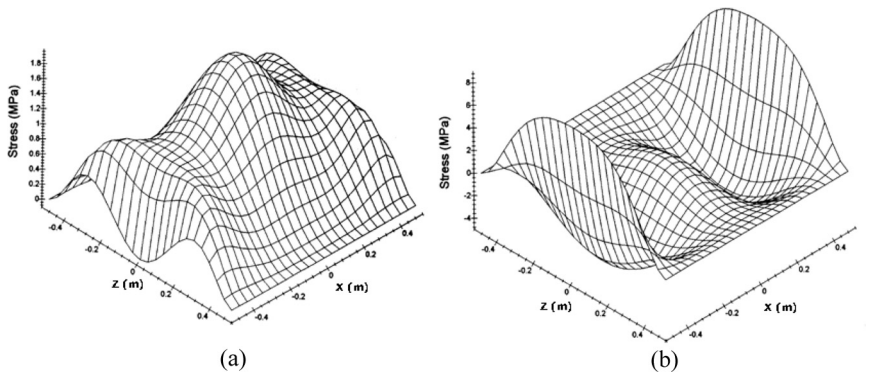

FIGURE 10 Stress σ_{zz}, (a) on the epoxy adhesive (Body B) and (b) on the aluminum substrate (Body A) at the spherical bi-material interface, as calculated by the mathematical procedure.

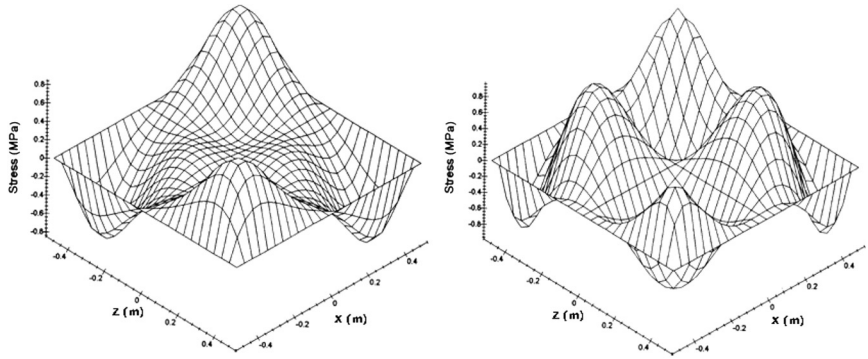

FIGURE 11 Stress σ_{xz}, (a) on the epoxy adhesive (Body B) and (b) on the aluminum substrate (Body A) at the spherical bi-material interface, as calculated by the mathematical procedure.

3.4. Comparison of Normal and Shear Stresses on Different Interfaces

In the theory of strength of materials, the normal stress and the shear stress play important roles in determining the conditions at which damage can occur.

Our mathematical procedure can easily provide the normal stress and shear stress on the interfaces.

For comparison purposes, the normal stresses on different interfaces are plotted in Fig. 13, and the shear stresses are plotted

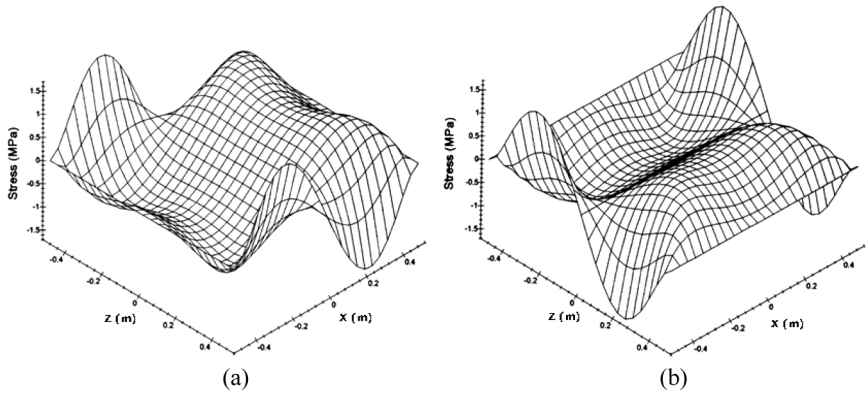

FIGURE 12 Stresses (a) σ_{xy} and (b) σ_{yz} on the epoxy adhesive (Body B) at the spherical bi-material interface, as calculated by the mathematical procedure.

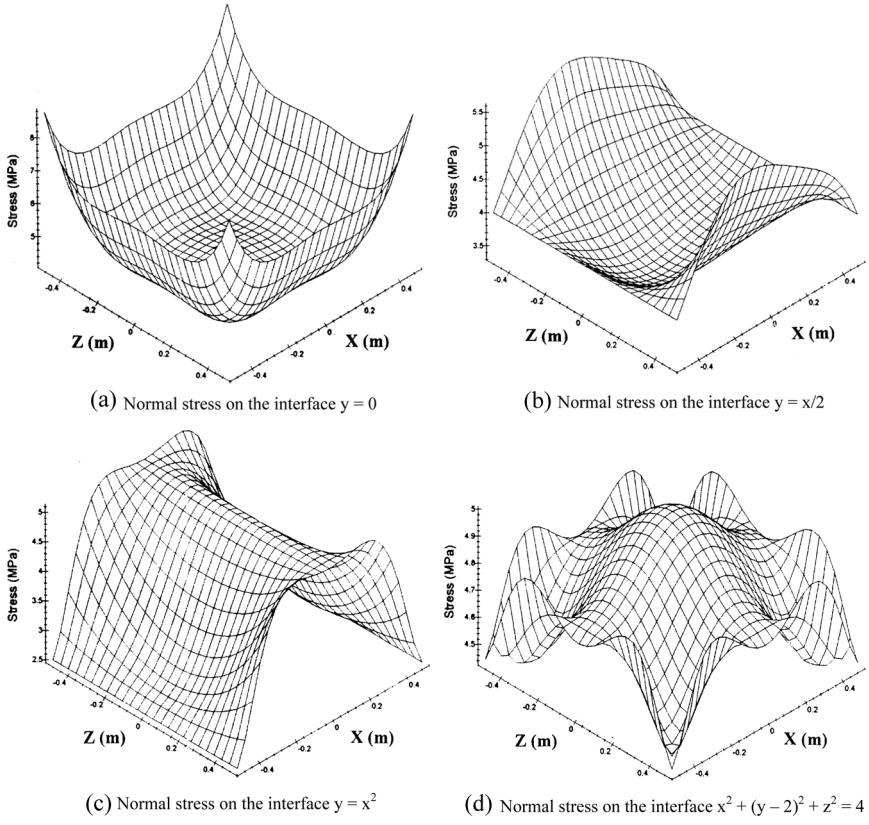

FIGURE 13 Normal stresses on different interfaces as calculated by the mathematical procedure.

in Fig. 14. As can be seen, the normal stress distributions are different on different interfaces. On the interface $y = 0$, the normal stress is maximum at the four comers. On the interface $y = x/2$, the maximum normal stresses are at the two edges, $z = \pm 0.5$. On the interface $y = x^2$, the maximum normal stresses are still on the two edges, $z = \pm 0.5$, but with about 10% less magnitude in comparison with the interface $y = x/2$. On the interface $x^2 + (y-2)^2 + z^2 = 4$, the normal stress has a peak at the center, as well as two peaks on each of the four edges. These peak values are rather close in magnitude and about 10% smaller than the peaks we observe on the interface $y = x^2$.

The (in-plane) shear stresses are also different on different interfaces. But they have one thing in common, that is, the maximum shear stresses are always near the corners. The slopes of the interfaces

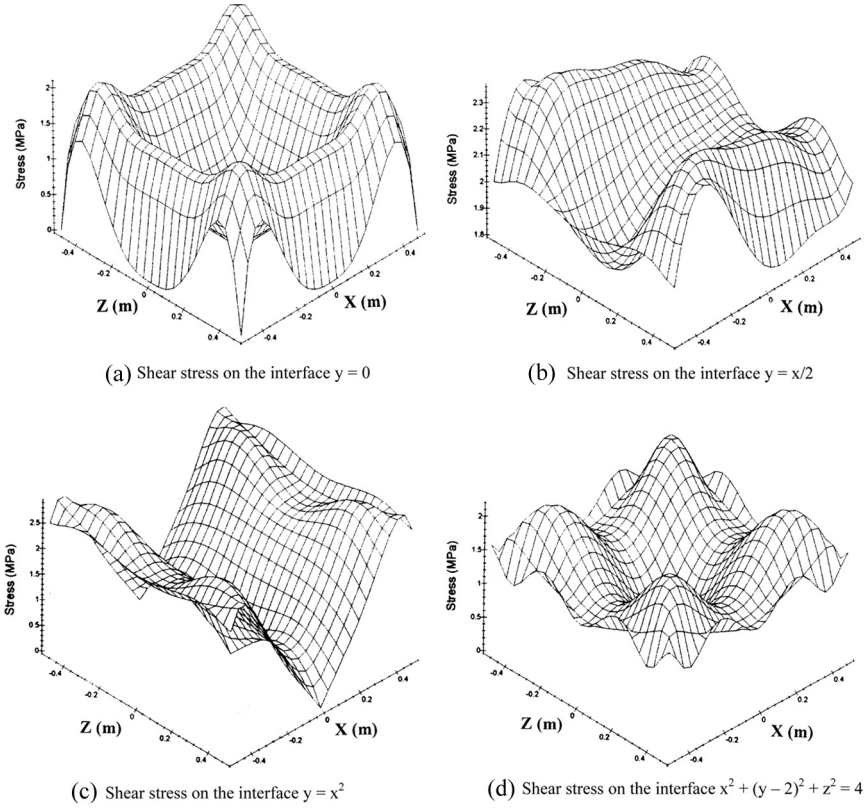

FIGURE 14 In-plane shear stresses on different interfaces as calculated by the mathematical procedure.

with the x-z plane determine the magnitudes of the maximum shear stresses. We note that in all four interfaces studied, only the shear stress peaks on the interface $y = x^2$ exceed 50% of the peak normal stress magnitudes, reaching approximately 56% of the normal stress along the z-axes shown in Figs. 13 and 14.

It is possible that, by changing the interfacial surface topography, an optimal interface can be found which will reduce the risk of interfacial damage caused by maximum normal stress and/or shear stress on the interfaces. Examination of Fig. 13 clearly reveals the flat interface, $y = 0$, as the most critical with highest normal stress magnitudes at each one of its four corners. Such stress peaks at corners are reduced significantly when the interface geometry is changed to those of scarf ($y = x/2$), parabolic ($y = x^2$), or spherical [$x^2 + (y - 2)^2 + z^2 = 4$]. In fact, nowhere on these three geometries do the normal stress

magnitudes exceed the peak values observed at the corners of the $y = 0$ surface. Further examination of Fig. 13 reveals the spherical surface as the most favorable of the four examined, since it has the lowest normal stress peaks, as well as (relatively) more uniform normal stress distribution. Examination of Fig. 14 reveals this finding to be true with the consideration of shear stress distribution on spherical interfaces as well.

4. CONCLUSIONS

The 3-D mathematical procedure we developed for obtaining the stress components at bonded bi-material interfaces offers significant promise in solving interface problems with different surface topographies, which can be described mathematically. Thus, the procedure developed provides an efficient tool to optimize interface construction by various methods such as chemical (etching), mechanical (machining, roughening, etc.), and other novel methods, such as laser ablation, currently becoming available to achieve a desired interface stress distribution for bonded materials. In this paper, using our procedure, we illustrated that the spherical surface is the most favorable in comparison with flat ($y = 0$), scarf ($y = x/2$), or parabolic ($y = x^2$) interfaces since it has the lowest normal and shear stress peaks, as well as having (relatively) more uniform stress distributions.

REFERENCES

[1] Adams, R. D. and Peppiatt, N. A., *J. Strain Anal.* **9**, 185 (1974).
[2] Cooper, P. A. and Sawer, J. W., A critical examination of stresses in an elastic single lap joint, (NASA Tech. Paper 150, National Technical Information Service, Springfield, VA, 1979).
[3] Dorn, L. and Weiping, L., *Intl. J. Adhesion Adhesives* **13**, 21–31 (1993).
[4] Papini, M., Fernlund, G., and Spelt, J. K., *Intl. J. Adhesion Adhesives* **14**, 5–13 (1994).
[5] Groth, H. L. and Nordlund, P., *Intl. J. Adhesion Adhesives* **11**, 204 (1991).
[6] Hashim, S. A., Cowling, M. J., and Winkle, I. E., *Intl. J. Adhesion Adhesives* **10**, 139–145 (1990).
[7] Bogy, D. B., *J. Appl. Mech.* **38**, 377–386 (1971).
[8] Bogy, D. B. and Wang, K. C., *Intl. J. Solids Structures* **7**, 993–1005 (1971).
[9] Bogy, D. B., *Intl. J. Solids Structures* **6**, 1287–1313 (1970).
[10] Bogy, D. B., *J. Appl. Mech.* **35**, 460–466 (1968).
[11] Groth, H. L., *Intl. J. of Adhesion Adhesives* **8**, 107–113 (1988).
[12] Ikegami, K., Takeshita, T., Matsuo, K., and Sugibayashi, T., *Intl. J. of Adhesion Adhesives* **10**, 199–206 (1990).
[13] Okajima, M. and Sinclair, G. B., in *SECTAM XIII Proceedings, The Southeastern Conference on Theoretical and Applied Mechanics*, W. F. Ranson and J. M. Biedenbech (Eds.), (Engineering Extension Service, Auburn Univ. AL, 1986), Vol. 2, pp. 367–371.

[14] Bigwood, D. A. and Crocombe, A. D., *Intl. J. of Adhesion Adhesives* **9**, 229–242 (1989).
[15] Ganghoffer, J. F. and Schultz, J., *J. Adhesion Sci. Technol.* **10**, 775–806 (1996).
[16] Renton, W. J. and Vinson, J. R., *J. Appl. Mech.* **45**, 101–106 (1977).
[17] Sancaktar, E., *Appl. Mech. Rev.* **40**, 1393–1402 (1987).
[18] Sancaktar, E., *Appl. Mech. Rev.* **49, Part 2**, S128–S138 (1996).
[19] Mittal, R. K. and McKenzie, H. W., *J. Adhesion* **11**, 91–104 (1980).
[20] Carpenter, W., *J. Adhesion* **35**, 55–73 (1991).
[21] Adams, R. D., *J. Adhesion* **30**, 219–242 (1989).
[22] Maugis, D., *J. Adhesion Sci. Technol.* **10**, 161–175 (1996).
[23] Keisler, C. and Lataillade, J. L., *J. Adhesion Sci. Technol.* **9**, 395–411 (1995).
[24] Gao, Z. and Mura, T., *Intl. J. Eng. Sci.* **29**, 685–692 (1991).
[25] Sih, G. C., *Polym. Eng. Sci.* **20**, 977–981 (1980).
[26] Chow, T. S., *J. Polym. Sci., Polym. Phys. Ed.* **16**, 959–965 (1978).
[27] Apalak, M. K., Davies, R., and Apalak, Z. G., *J. Adhesion Sci. Technol.* **9**, 267–293 (1995).
[28] Suhir, E., *J. Appl. Mech.* **55**, 143–148 (1988).
[29] Sancaktar, E. and Narayan, K., *J. Adhesion* **13**, 237–271 (1999).
[30] Sawa, T., Temma, K., and Ishikama, H., *J. Adhesion* **31**, 33–43 (1989).
[31] Temma, K., Sawa, T., and Tsunoda, Y., *J. Adhesion* **10**, 294–300 (1990).
[32] Nakano, Y., Temma, K., and Sawa, T., *J. Adhesion* **34**, 137–151 (1991).
[33] Temma, K., Sawa, T., Uchida, H., and Nakano, Y., *J. Adhesion* **33**, 133–147 (1991).
[34] Sawa, T., Temma, K., Nishingaya, T., and Ishikawa, H., *J. Adhesion Sci. Technol.* **9**, 215–236 (1995).
[35] Sancaktar, E., Lipshitz, H., Babu, S. V., Zhang, E., and D'Couto, G. C., *J. Adhesion* **50**, 103–133 (1995).
[36] Sancaktar, E., *J. Adhesion Sci. Technol.* **9**, 119–147 (1995).
[37] Penado, F. E. and Dropek, R. K., in *ASM Engineered Materials; Vol. 3; Adhesives and Sealants*, H. F. Brinson (Technical Chairman), (ASM International, Materials Park, OH, 1990), pp. 477–500.
[38] Dropek, R. K., in *ASM Engineered Materials Handbook, Vol. 1, Composites*, T. J. Reinhart (Technical Chairman) (ASM International, Materials Park, OH, 1987), pp. 463–478.
[39] Baylor, S. J. and Sancaktar, E., in *Reliability, Stress Analysis, and Failure Prevention Issues in Emerging Technologies and Materials*, E. Sancaktar (Ed.), (ASME, New York, 1995), DE-Vol. 87, pp. 41–48.
[40] Ma, W., Gomatam, R., Fong, R., and Sancaktar, E., *J. Adhesion Sci. Technol.* **15**, 1533–1558 (2001).
[41] Ma, W., Gomatam, R., and Sancaktar, E., *J. Adhesion Sci. Technol.* **17**, 831–846 (2003).
[42] Sancaktar, E. and Gomatam, R., *J. Adhesion Sci. Technol* **15**, 97–117 (2001).
[43] Struik, D. J., *Classical Differential Geometry*, (Addison-Wesley, New York, 1950). pp. 50, 73, 124.
[44] Washizu, K., *J. Mathematics and Physics* **36**, 306–312 (1958).
[45] Washizu, K., *Variational Methods in Elasticity and Plasticity*, (Pergamon Press, New York, 1982).
[46] Fung, Y. C., *Foundations of Solid Mechanics*, (Prentice-Hall, Englewood Cliffs, NJ, 1965).
[47] Hildebrand, F. B., *Advanced Calculus for Applications*, (Prentice-Hall, Englewood Cliffs, NJ, 1962).
[48] Reklaitis, G. V., Ravindran, A., and Ragsdell, K. M., *Engineering Optimization*, (John Wiley, New York, 1983).